



# A study on the effect of vibration parameters on the shot velocity in SMAT process using dynamic finite element analysis

E. Yazar\* and A. Tamer Ertürk

*Department of Mechanical Engineering, Kocaeli University 41380, Kocaeli, Turkey.*

Received 18 April 2021; received in revised form 10 September 2021; accepted 7 March 2022

## KEYWORDS

SMAT;  
 Shot velocity;  
 Vibration frequency;  
 Vibration amplitude;  
 FEM.

**Abstract.** In this study, factors affecting average shot velocity in the Surface Mechanical Attrition Treatment (SMAT) process were investigated numerically. The numerical model was developed by using the finite element method. The effects of frequency, amplitude, and projection distance parameters on shot velocity were simulated. Response Surface Methodology (RSM) was used to evaluate the simulation results. ANOVA tables were used for statistical evaluation. Moreover, the regression equations derived from simulation results were compared with the theoretical equations. Besides, the effect of the amount of shot in the SMAT chamber on the velocity of the shot is simulated. The results showed that apart from frequency and amplitude, projection distance also had a significant impact on shot velocity.

© 2022 Sharif University of Technology. All rights reserved.

## 1. Introduction

Ultrasonic Shot Peening (USP) is a mechanical surface treatment applied to metallic materials. Surface Mechanical Attrition Treatment (SMAT) is the name given to USP in the literature [1]. During the SMAT process, high-frequency ultrasonic vibration induces multi-directional spherical shots with high kinetic energy in a closed chamber. These spherical shots collide with a sample surface several times [2,3]. The SMAT process has some similarities with Conventional Shot Peening (CSP) [4]. While shot velocity is between 1 – 20 m/s in SMAT [5], it is usually between 20 – 100 m/s in CSP [6,7]. Many disparate factors affect

shot velocity in SMAT: specimen-sonotrode distance, shot quantity, amplitude, vibration frequency of the sonotrode, and the geometry of a chamber. Because of the microstructural and mechanical properties that are expected to change depending on the shot velocity, the shot velocity is the most critical parameter to determine in the SMAT treatment. The height and diameter of the SMAT chamber directly affect the shot velocity. As a result, adopting a suitable chamber design is critical for achieving the desired mechanical properties of the target material. Due to enormous strains and high strain rates at relatively low temperatures, the SMAT process exposes the target material's surface to severe plastic deformation, resulting in ultrafine-grain or nanostructure forms [8,9]. The plastic deformation mechanism is activated by the twinning, dislocation, and grain boundary sliding mechanisms. Dislocations are very effective in the development of plastic deformation microstructures, which can be measured using structural parameters such as high angle and misorientations along dislocation boundaries, as well as

\*. Corresponding author. Tel.: +905542160574  
 E-mail addresses: [e.yazar@kocaeli.edu.tr](mailto:e.yazar@kocaeli.edu.tr),  
[eser.yazar@kocaeli.edu.tr](mailto:eser.yazar@kocaeli.edu.tr) (E. Yazar);  
[tamer.erturk@kocaeli.edu.tr](mailto:tamer.erturk@kocaeli.edu.tr) (A. Tamer Ertürk)

spacing between boundaries [10,11]. SMAT increases intragranular misorientation from the peened surface to depth [12]. Compressive residual stresses also occur in the area affected by SMAT [8]. These compressive residual stresses associated with grain refinement of the microstructure delay the initiation and propagation of fatigue cracking and increase the fatigue resistance of the material [13]. In addition, when compared to conventional peening methods, SMAT causes slight roughness on the material surface. Excessive roughness can have a negative impact on wear resistance and accelerates the initiation and propagation of cracks. To get 100% coverage in the SMAT treatment, some time is required. The coverage rate is very significant, especially for residual stress and surface roughness measurements [14].

In SMAT processes, the shots impact a surface of material randomly with the effect of vibration. Besides, the shots incoherently collide with each other and the inner surface of the chamber. As a result of these collisions, the speed of each shot varies continuously inside the vibration chamber. Therefore, determining the shot velocity becomes a complex phenomenon, especially in numerical and analytical studies. For this reason, many researchers assumed the shot velocity as average velocity in SMAT. For the vibration chamber, Todaka et al. chose an amplitude of 90  $\mu\text{m}$ , a frequency of 20 kHz, and a projection distance of 10 mm, claiming that the shot speed could be less than 20 m/s [6]. Using a piezoelectric transducer actuating at 20 kHz, Chaise et al. determined the sonotrode amplitude to be 25  $\mu\text{m}$  and the height of the vibration chamber to be 50 mm. For the numeric model, they specified the Average Shot Velocity (ASV) to be 4 m/s [15]. Astarae et al. calculated the ASV in the vibration chamber as 3.6 m/s to use it in the numerical model in a specially designed experimental setup [16]. Yin et al. assumed an ASV of 3.6 m/s in their study [17]. Manchoul et al. determined the ASV to be 4 and 8 m/s for two different amplitudes of 32 and 64  $\mu\text{m}$  and a constant frequency of 20 kHz [18]. Smaller peening distances result in higher impact energy, while longer peening distances result in lower impact energy, according to Sun et al. [19]. These and other similar studies involve a theoretical calculation of the ASV. In SMAT, the vibration signal generated by the ultrasonic generator is in the form of a harmonic sinusoidal function:

$$x(t) = A \sin \omega t, \quad (1)$$

$$\omega = 2\pi f, \quad (2)$$

where  $A$  is the amplitude of vibration,  $\omega$  is the pulsation and  $f$  is the frequency of sonotrode. The first-order derivative of  $x(t)$  is:

$$\frac{dx}{dt} = A\omega \cos \omega t. \quad (3)$$

Eq. (3) is used to calculate the maximum initial velocity:

$$V_{i,\max} = 2A\pi f. \quad (4)$$

Some researchers studied shot dynamics in SMAT. Du et al. reported that the vibration frequency increases the shot velocity. They also indicated the frequency-dependent velocity of the vibration chamber and the change of shot velocity [20]. Pilé et al. suggested a model for the interaction between shot & sonotrode and reported that the ASV could increase as the shot quantity decreases. They also stated that increased vibration amplitude could increase the shot velocity, but increased interaction speed could increase the dissipated energy [21]. Micoulaut et al. developed the Event-Driven-Dynamics algorithm, based on the granular gas model, to understand the shot dynamics, which has a complex structure in the USP [22]. Based on the same algorithm, Badreddine et al. investigated the effect of sonotrode amplitude, vibration chamber geometry and shot diameter on shot dynamics [23]. Rousseau et al. investigated experimentally and numerically how the shot quantity affects the surface properties in SMAT. They determined the ASV for a numerical model using the Discrete Element Method (DEM). For SMAT, they used a frequency of 20 kHz, a half-amplitude (0 - peak) of 4  $\mu\text{m}$ , and a distance of 30 mm between the sample and the sonotrode. They reported that the increase in the shot quantity reduced the ASV [24].

The literature review has shown that there are a limited number of studies on shot dynamics for SMAT. These studies were carried out with the Event-Driven-Dynamics algorithm, which is adapted to the granular gas model, and DEM. Shot velocity is one of the most important parameters that directly affect the results of SMAT such as nanocrystalline layer [25–27], fatigue strength [28–30], corrosion resistance [31–34], wear resistance [35–38] etc. Especially for numerical studies, it is remarkable to determine the shot velocity accurately. The purpose of our study is to reveal how SMAT parameters affect ASV. The Finite Element Method (FEM) was used to reveal the effect of vibration frequency and amplitude, vibration chamber dimension and shot quantity on shot velocity. Numerical simulations were performed using ANSYS/AUTODYN explicit dynamics solver. In addition, based on the simulation results, statistical analyses of shot velocity were made.

## 2. Dynamic finite element analysis

SMAT is a process applied at frequencies above 20 kHz. On the other hand, many shots collide randomly with each other and the vibration chamber, coincidentally. A shot in the SMAT process gains kinetic energy at the

start of the vibration application that can cause a continuous energy transfer within the vibration chamber due to the collisions and contacts. ANSYS/Explicit Dynamics module is designed to simulate particular purposes such as low-high velocity impacts, complex contact conditions, high-frequency dynamic response, etc. It is also very suitable for simulations in a short time such as the SMAT process where there are countless collisions in an ultrashort time. Therefore, shot dynamics simulations for SMAT were carried out using ANSYS/Explicit Dynamics.

**2.1. Finite element model**

The vibration chamber in the simulations is composed of a closed and hollow cylinder, as well as shots, just like in the experiments. The diameters of the cylinder and the shot were 8.5 and 3 mm, respectively. A total of 21 shots were placed in the vibration chamber to provide complete coverage of the lower surface of the cylinder. To reduce the time of simulation, both the cylinder and shots are defined as surface bodies. The vibration chamber and shots were defined as stainless steel, and the isotropic elastic material model was used for both in the simulations. Table 1 shows the material properties of stainless steel. Here, the density for stainless steel was  $7.75 \text{ g.cm}^{-3}$ , the elasticity modulus was 193 GPa and the Poisson's ratio was

0.31. The stiffness behavior of all the materials was considered to be completely rigid.

Each shot's body interaction was defined as distinct and independent from the interactions of the other shots and chamber surfaces. Frictions were ignored since all contacts between the surfaces were chosen as frictionless sliding contacts. The meshing element size was 0.25 mm, and the Quad/Tri rigid mesh face type was used. Figure 1 exhibits the mesh structure generated for the FE model. Ultrasonic vibration was defined as a harmonic sinusoidal function for the vibration chamber. Dissimilar vibration chambers (5, 10, 20 mm) were designed for determining effects on the shot velocity of changing distance between the shot and the upper surface of the cylinder. Accordingly, at different heights of the vibration chambers, the projection distances were 2, 7, 17 mm. The projection distance is the span between the top point of a spherical shot and the sample surface. Table 2 presents all vibration parameters selected for simulations. Figure 1 displays the schematic view of the model created for FE. The

**Table 1.** Isotropic elastic material model of stainless steel.

Density ( $\text{g.cm}^{-3}$ )	Elasticity modulus (GPa)	Poisson's ratio
7.75	193	0.31

**Table 2.** Selected factors and levels of simulations.

Factors	Levels	Values
Amplitude ( $\mu\text{m}$ )	3	25; 50; 100
Frequency (kHz)	3	20; 30; 40
Distance (mm)	3	2; 7; 17

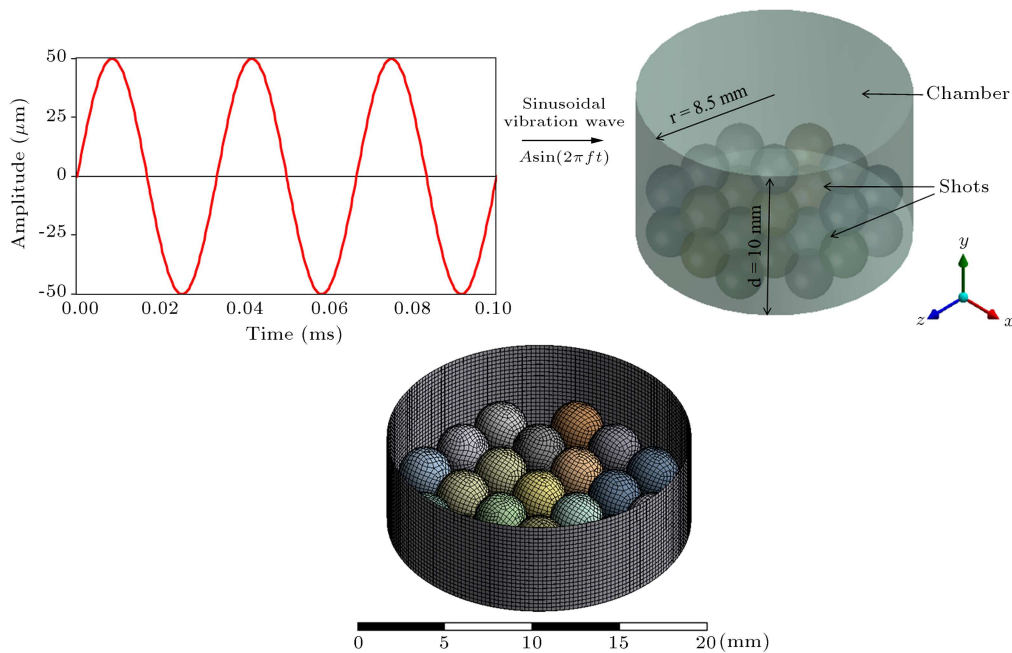


**Figure 1.** Schematic view of FE model.

mesh structure and 3D view of the vibration chamber, as well as shots, are detailed here. In addition, the amplitude and frequency graph of the sinusoidal vibration wave ( $A\sin 2\pi ft$ ) applied to the vibration chamber is also shown. In general, Figure 1 aims to demonstrate the implementation of the finite element model. The total simulation time for each analysis was 10 ms. Temperature changes after collisions were neglected.

### 2.2. Statistical analysis

Statistical methods were chosen to evaluate the simulation results in this study. Minitab 19 statistical software was used to evaluate experimental results using Response Surface Methodology (RSM). Frequency, amplitude, and distance were all defined as continuous factors during the model's development. The simulations were planned according to the Box-Behnken design for surface response as shown in Table 3. The relationship between the independent variables and the responses in RSM is defined by a second-order polynomial model given below:

$$y = \beta_0 + \sum_{i=1}^k \beta_i x_i + \sum_{i=1}^k \beta_{ii} x_i^2 + \sum_{i=1}^{k-1} \sum_{j=2}^k \beta_{ij} X_i X_j + \varepsilon, \quad (5)$$

where  $y$  is predicted response,  $\beta_0$  is constant and  $\beta_i$ ,  $\beta_{ii}$ , and  $\beta_{ij}$  represent coefficients of linear, quadratic, and interaction terms, respectively. While  $X$  shows the coded variables,  $\varepsilon$  indicates the error [8,39]. The simulation results were subjected to a variance analysis with a 95% confidence interval for  $P$  values [40,41].

## 3. Results

A total of 14 separate simulations were performed based on the experimental design of the RSM. Shot velocity was continuously changing during the simulation due to the effects of collisions and vibration. Figure 2 shows the velocity graph obtained during the simulation of one shot. During the simulation, the lowest shot velocity was achieved. Figure 3 shows the total velocity contours obtained at the same frequencies and amplitudes ( $50 \mu\text{m}$ , 30 kHz). Due to the vibration, the shot velocity reached roughly 9.3 m/s and remained constant for the first 1 ms. When it collided with other shots and the vibration chamber's surfaces, it tended to increase and decrease. For example, the shot was subjected to low-energy collisions between 2 and 3 ms. However, these collisions could not significantly change the shot velocity. When the shot came in contact with the chamber's bottom surfaces, it reached its maximum velocity. Thus, the shot velocity profile is similar to the

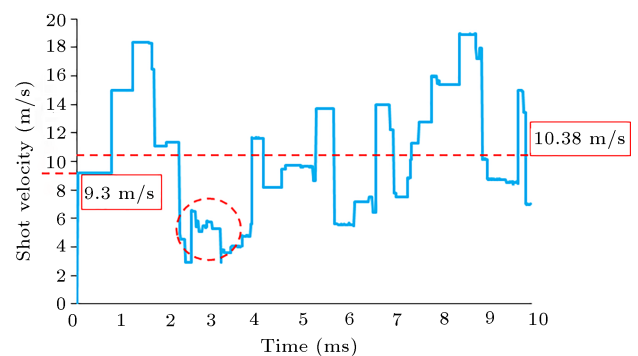
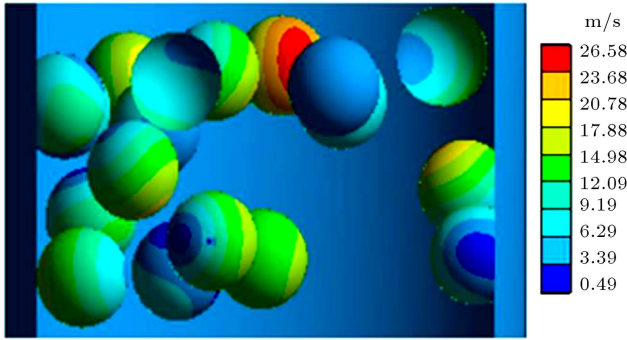


Figure 2. Average velocity of one-shot ( $50 \mu\text{m}$ , 30 kHz, 10 mm).

Table 3. Total velocity results of all SMAT simulations.

Factors			Shot velocity (m/s)		
Amplitude ( $\mu\text{m}$ )	Frequency (kHz)	Distance (mm)	Average	Maximum	Minimum
25	20	10	3.74	4.92	2.89
100	20	10	13.51	16.31	11.38
25	40	10	6.35	8.51	4.99
100	40	10	23.26	27.05	19.31
25	30	5	5.73	7.97	3.78
100	30	5	19.56	24.22	17.97
25	30	20	4.65	5.82	3.92
100	30	20	16.62	21.34	13.73
50	20	5	7.99	9.88	6.46
50	40	5	13.33	15.74	11.70
50	20	20	5.95	7.68	3.80
50	40	20	10.04	12.44	7.67
50	30	10	9.52	11.80	5.82
50	20	10	6.69	7.92	5.65



**Figure 3.** Total velocity contours (50  $\mu\text{m}$ , 30 kHz, 10 mm).

sinus function. For statistical analysis, the ASV was obtained by averaging this graph. For instance, the mean speed of a shot was calculated to be 10.384 m/s, as shown in Figure 2.

Table 3 shows the ASV results calculated according to each simulation. ASV has been calculated by taking the mean of all 21-shot velocities. The highest and lowest shot velocities of each case during the simulation time are given in the same table.

**3.1. Analysis of variance**

Table 4 shows the results of the variance analysis for the ASV. When the *P*-value is evaluated within the 95% confidence interval, it is seen that all three factors had a significant effect on the average velocity linearly.

ANOVA tables obtained for maximum and minimum shot velocities are given in Tables 5 and 6. When examined for the maximum shot velocity, the *P*-value (0.06) obtained for the distance was outside the confidence interval. Likewise, the *P*-value for the distance is calculated as  $0.05 < 0.44$  within the minimum shot velocity and remained outside the confidence interval.

**Table 4.** ANOVA of average shot velocity.

Source	DF	Contribution	Adj SS	Adj MS	F-value	P-value
Model	9	99.89%	461.547	51.283	406.51	0.000
Linear	3	96.61%	248.430	82.810	656.42	0.000
<i>A</i>	1	79.92%	203.166	203.166	1610.46	0.000
<i>F</i>	1	14.36%	39.956	39.956	316.73	0.000
<i>D</i>	1	2.33%	2.468	2.468	19.56	0.011
Square	3	0.06%	0.398	0.133	1.05	0.462
<i>A</i> <sup>2</sup>	1	0.00%	0.038	0.038	0.30	0.612
<i>F</i> <sup>2</sup>	1	0.02%	0.012	0.012	0.10	0.773
<i>D</i> <sup>2</sup>	1	0.04%	0.245	0.245	1.94	0.236
2-way interaction	3	3.23%	14.903	4.968	39.38	0.002
<i>AF</i>	1	2.97%	13.464	13.464	106.73	0.000
<i>AD</i>	1	0.16%	0.731	0.731	5.80	0.074
<i>FD</i>	1	0.10%	0.445	0.445	3.53	0.134
Error	4	0.11%	0.505	0.126		
Total	13	100.00%				

$R^2 = 99.89\%$ ;  $R^2(\text{adj}) = 99.65\%$ ;  $R^2(\text{pred}) = 98.32\%$

**Table 5.** ANOVA of maximum shot velocity.

Source	DF	Contribution	Adj SS	Adj MS	F-value	P-value
Model	9	99.87%	638.431	70.937	343.66	0.000
Linear	3	97.06%	354.733	118.244	572.85	0.000
<i>A</i>	1	80.86%	297.934	297.934	1443.39	0.000
<i>F</i>	1	14.25%	52.547	52.547	254.57	0.000
<i>D</i>	1	1.94%	1.391	1.391	6.74	0.060
Square	3	0.52%	3.656	1.219	5.90	0.060
<i>A</i> <sup>2</sup>	1	0.10%	0.473	0.473	2.29	0.205
<i>F</i> <sup>2</sup>	1	0.26%	0.543	0.543	2.63	0.180
<i>D</i> <sup>2</sup>	1	0.16%	1.176	1.176	5.70	0.075
2-Way Interaction	3	2.29%	14.660	4.887	23.67	0.005
<i>AF</i>	1	2.22%	13.912	13.912	67.40	0.001
<i>AD</i>	1	0.00%	0.030	0.030	0.15	0.720
<i>FD</i>	1	0.07%	0.445	0.445	2.16	0.216
Error	4	0.13%	0.826	0.206		
Total	13	100.00%				

**Table 6.** ANOVA of minimum shot velocity.

Source	DF	Contribution	Adj SS	Adj MS	F-value	P-value
Model	9	98.92%	377.798	41.978	40.71	0.001
Linear	3	94.77%	176.649	58.883	57.11	0.001
A	1	78.53%	146.803	146.803	142.38	0.000
F	1	12.77%	27.687	27.687	26.85	0.007
D	1	3.47%	0.743	0.743	0.72	0.444
Square	3	0.95%	3.852	1.284	1.25	0.404
A <sup>2</sup>	1	0.20%	2.097	2.097	2.03	0.227
F <sup>2</sup>	1	0.02%	0.791	0.791	0.77	0.430
D <sup>2</sup>	1	0.73%	2.935	2.935	2.85	0.167
2-Way Interaction	3	3.21%	12.256	4.085	3.96	0.108
AF	1	2.33%	8.738	8.738	8.47	0.044
AD	1	0.81%	3.095	3.095	3.00	0.158
FD	1	0.07%	0.266	0.266	0.26	0.638
Error	4	1.08%	4.124	1.031		
Total	13	100.00%				

These results indicate that the effect of distance on the maximum and minimum shot velocities is not significant. However, frequency and amplitude factors have a powerful influence on maximum and minimum shot velocities.

### 3.2. Shot velocity evaluation

Figure 4 shows the main effect plots obtained for shot velocities. The main effect plots obtained for the

maximum and minimum shot velocities are given in Figure 4(a) and (b), respectively. The shot velocity increases with increasing amplitude and frequency, as shown in both graphs. The maximum shot velocity is more variable than the minimum shot velocity. Besides, ANOVA tables reveal that the plot obtained for distance was not significant. Figure 4(c) shows the main effect plot of the ASV. The frequency and amplitude directly increase the shot velocity. Frequency and

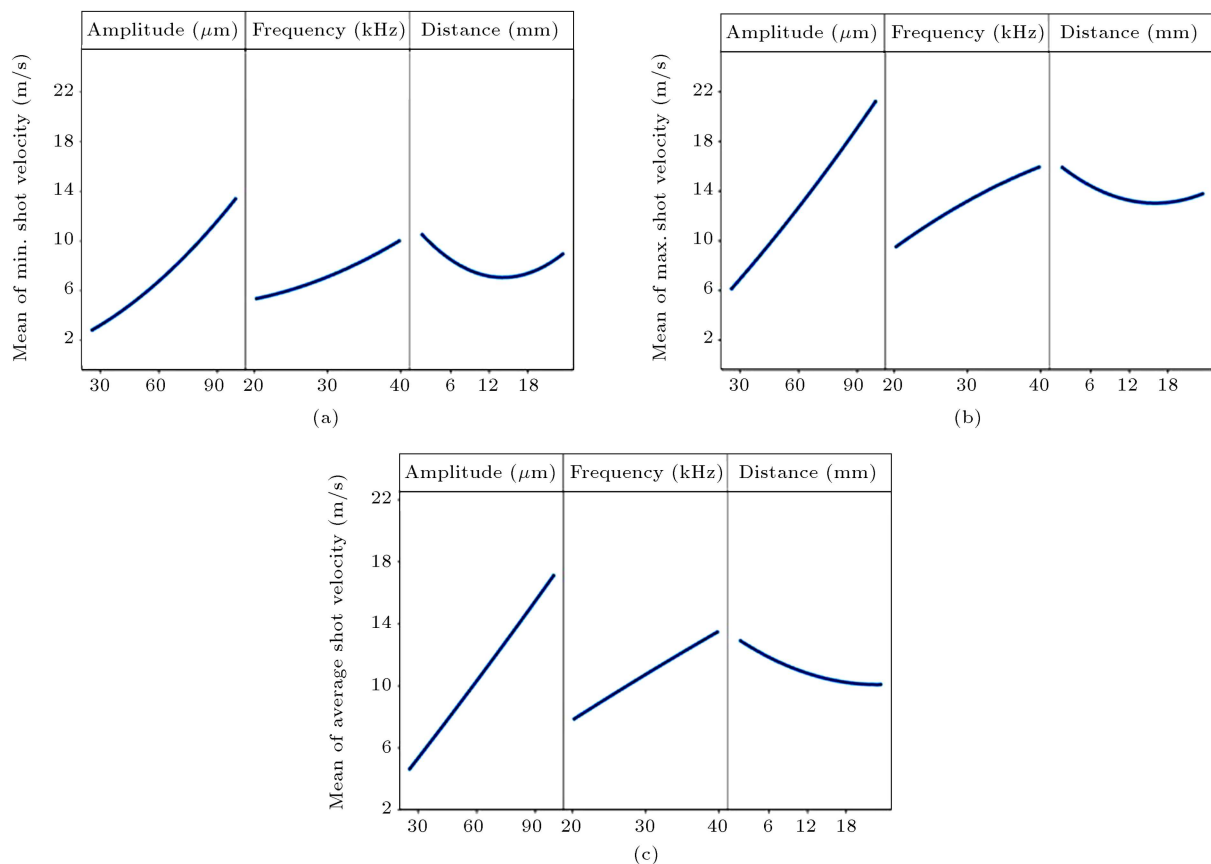


**Figure 4.** Mean plots of shot velocity (m/s): (a) Min. shot velocity, (b) max. shot velocity, and (c) avg. shot velocity.

amplitude directly affect the kinetic energy transferred to the shot. These results are in agreement with the literature [20]. Shot velocity decreased as the distance between the shot and the chamber’s upper surface (projection distance) increased. The effect of this reduction on ASV (2.33%) was not as high as frequency and amplitude. However, as mentioned earlier, the shot velocity is probably the most decisive parameter in SMAT. Therefore, even low effects are considered in terms of process efficiency.

The amount of kinetic energy transferred to the shot increased as the vibration amplitude and frequency increased. Increased kinetic energy causes an increase in shot velocity. However, there is a different phenomenon. Namely, as the interaction speed between the shots increases, the dissipation of energy will increase. The shot velocity will be reduced as a result of this situation. Simulation results revealed that the average shot velocity increased with vibration frequency and amplitude. However, increasing projection distance caused a decrease in ASV. The shot velocity reached the maximum level in the case where the distance was the lowest. Low-distance caused the shot to collide with the sonotrode in shorter times. The sonotrode kinetic energy could be transferred to the shots without causing an increase in energy dissipation. As the distance increases, the contact time of the shots with the sonotrode, that is, the time to regain kinetic energy will decrease. This condition could enhance the interaction between shots, as well as the energy dissipation, and lower the ASV. Figure 5 shows the average velocity’s contour graph. Frequency and amplitude increase the average velocity almost equally. Besides, increasing distance increases the area of low-velocity regions. However, as the amplitude increases, the distance effect decreases because it increases the shot velocity.

**3.3. Effect of shot quantity**

Shots completely covered the lower surface of the vibration chamber, which had been designed in all simulations up to this point in the study. In this phase,

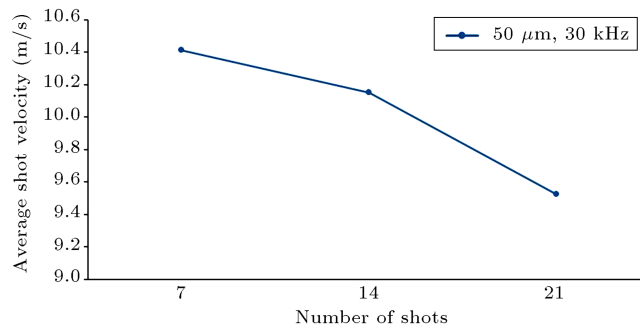


**Figure 6.** Number of shots - average shot velocity (m/s).

the number of shots was gradually lowered from 21 to 14, and then to 7. The ASV was then simulated. The other vibration parameters were kept constant at 50 μm, 30 kHz, and 10 mm. The effects of shot quantity on shot velocity are depicted in Figure 6. Accordingly, the increase in the shot quantity reduced the shot velocity. When compared to 21 shots, the shot velocity of 7 shots is dropped by 8.5%. As the number of shots increased, so did the interaction between them, resulting in an increase in energy dissipation. This situation causes the shot velocity to decrease. This result confirms the previous studies [24].

**3.4. Regression equations**

After evaluating the simulation results for ASV according to RSM, the regression equation could be given as follows:

$$ASV(m/s) = 0.08 + 0.0319A + 0.086F - 0.062D + 0.0001A^2 - 0.00072F^2 + 0.0062D^2 + 0.0048AF - 0.0015AD - 0.00432FD, \quad (6)$$

where A is the amplitude (μm), F is the frequency (kHz) and D (mm) is the projection distance, respectively. R<sup>2</sup> indicates a regression equation’s ability to estimate simulation results. Predicted R<sup>2</sup> shows the ability to predict possible observations using a regression equation [8]. R<sup>2</sup> and R<sup>2</sup> (pred) values for ASV are 99.89% and 98.32% (Table 4), respectively. As can be seen, the established model’s success in

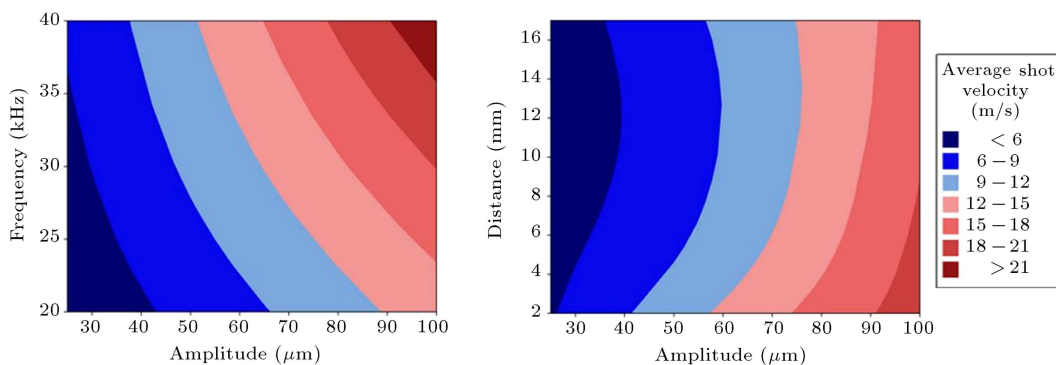


**Figure 5.** Contour plots of average shot velocity.

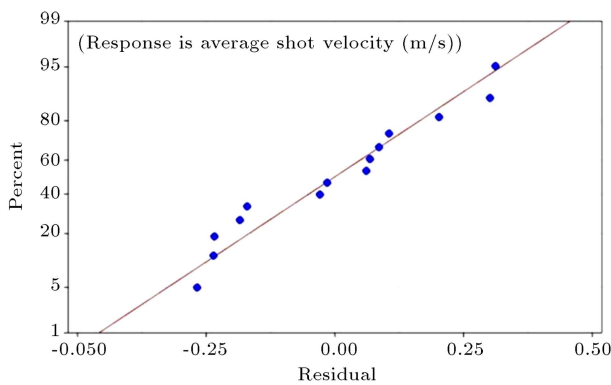


**Figure 7.** Normal probability plot of average shot velocity.

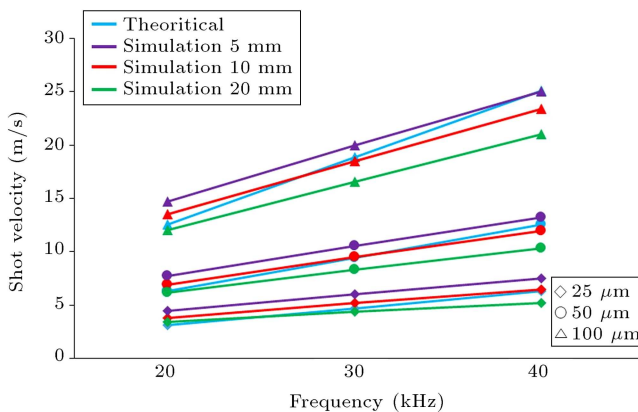


**Figure 8.** Comparative shot velocity results from theoretical and simulation.

predicting simulation results is sufficient. The normal probability plot for the ASV is shown in Figure 7.

Eq. (6) shows modelling findings for frequency, amplitude, and distance-dependent shot velocity based on simulation data. Eq. (4) calculates the theoretical shot velocity based on frequency and amplitude. Figure 8 compares the results of both equations' shot velocity calculations. Eq. (6) can predict the shot with high accuracy depending on the distance, as shown in Figure 8. In addition, at varying chamber heights, this figure shows fairly consistent shot velocity values (5, 10, 20 mm). The results of the investigation, with a projection distance of 7 mm, are very similar to theoretical calculations. However, changing the projection distance changed the shot velocity. As previously stated, the decrease in shot velocity has been caused by the increase in projection distance.

#### 4. Discussion

The multiple and vibration-induced collisions in Surface Mechanical Attrition Treatment (SMAT) result in a complicated contact interaction. The aim was to develop a general approach to momentum conser-

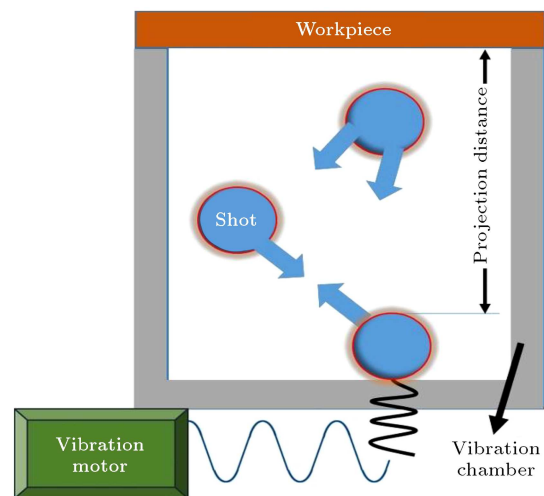


**Figure 9.** Schematic illustration of the analytical approaches.

vation that could be applied to shot-shot and shot-chamber surface interactions. However, thermal effects and friction factors are neglected in these analytical approaches.

Figure 9 exhibits a schematic illustration of the analytical approaches. In this study, the shot-shot interaction system consists of  $N = 21$  shots. Each shot interacts with another shot via action/reaction pairs of forces. Moreover, each shot is subjected to vibrational forces from the chamber and workpiece. To understand the messy details of collisions in SMAT, basic mechanic models must be used to simplify them. The momentum of a shot velocity is calculated by multiplying mass and speed. The total momentum of the shot-shot interaction system is the vector sum of the individual momentum. The total momentum's time derivative informs us about how the system's momentum changes over time. Vibrational forces from the chamber surface or workpiece, as well as interaction forces from all other shots in the system, make up the net force acting on a shot. The shot-shot interaction forces are distributed in action/reaction pairs, with the sum of all shot-shot interaction forces equal to zero. The chamber surface or workpiece exerts the net force of a shot on the system. According to Newton's second law, the overall momentum of the shot-shot interaction system changes at the same rate as the net force applied to it. The critical implication is that the motion in the SMAT process can be analyzed without needing to consider shot-shot interaction forces. The net external force is not zero thus the SMAT process is not an isolated system. Therefore, the total momentum is unconstant. Solely Newton's law of conservation of momentum is insufficient to evaluate the SMAT process. Some of the mechanical energy is dissipated as thermal energy inside the shots during the process. Thus, all of the kinetic energy is not recovered. Besides, some of

the mechanical energy is stored as elastic potential energy in compressed molecular bonds. Kinetic energy is stored as elastic potential energy in compressed molecular bonds, and then all of the stored energy is transformed back into the post-collision kinetic energy of the objects. If mechanical energy after a collision is conserved, a perfectly elastic collision can happen. A shot is a very hard steel object so that it comes close to being perfectly elastic. The kinetic energy of the shots can be calculated based on the elastic collision between the shots and the chamber surface. The vibration motion in the SMAT process has a harmonic longitudinal character and can be characterized using angular velocity. The vibration motor velocity ( $\nu_m$ ) can be calculated using the motor frequency ( $f_m$ ) and angular velocity ( $\omega_m$ ) as below:

$$\nu_m = \omega_m \sin(2\pi f_m t). \quad (7)$$

The initial speed of a shot ( $\nu_0$ ) at the bottom surface of the chamber before the second collision can be represented as below:

$$\nu_{0,s} = \frac{2A\omega_m}{1 + \frac{m_s}{m_c+m}} \sin \phi, \quad (8)$$

where  $m_s$  is the mass of a shot,  $m_c + m$  is the sum of motor and chamber mass, and  $\phi$  is the phase of harmonic vibration. A collision between shot-chamber surface and shot-workpiece happens under the following condition:

$$\frac{1}{2} m \nu_{0,s}^2 > mgd_p, \quad (9)$$

where  $d_p$  is the projection distance, and  $g$  is the gravitational acceleration. During the collision, the impulsive force acts for a short period and transforms its kinetic energy into deformation or thermal energy. Other forces, such as friction or gravity, are negligible in comparison to the impulsive force, so the impulse approximation is valid.

## 5. Conclusions

To determine the average shot velocity, the Surface Mechanical Attrition Treatment (SMAT) process was simulated using FEM modelling. The following are the findings of this study, which were used to determine the factors that affect shot velocity in SMAT processes:

- Distance has a significant effect on the average shot velocity along with frequency and amplitude;
- The distance has no significant effect on the maximum and minimum shot velocities;
- Increasing the number of shots in the SMAT chamber decreases the average shot velocity;
- A regression equation based on frequency, amplitude, and distance has been developed.

## Declaration of interests

The authors declare that they have no known competing financial interests or personal relationships that could have appeared to influence the work reported in this paper.

The authors declare the following financial interests/personal relationships which may be considered as potential competing interests.

## Nomenclature

SMAT	Surface Mechanical Attrition Treatment
ANOVA	Analysis of Variance
FEM	Finite Element Method
USP	Ultrasonic Shot Peening
CSP	Conventional Shot Peening
ASV	Average Shot Velocity (m/s)
DEM	Discrete Element Method
$x(t)$	Harmonic sinusoidal function ( $\mu\text{m}$ )
$A$	Amplitude of vibration ( $\mu\text{m}$ )
$\omega$	Pulsation (rad/s)
$f$	Frequency of sonotrode (Hz)
$V_{i,\text{max}}$	Maximum initial velocity of chamber (m/s)
$\nu_m$	Vibration motor velocity (m/s)
$\omega_m$	Angular velocity (rad/s)
$f_m$	Vibration motor frequency (Hz)
$\nu_{0,s}$	Initial speed of a shot (m/s)
$m_s$	Mass of a shot (gr)
$m_c + m$	Sum of motor and chamber mass (gr)
$\phi$	Phase of harmonic vibration
$d_p$	Projection distance (mm)
$g$	Gravitational acceleration ( $\text{m/s}^2$ )
RSM	Response Surface Methodology
$y$	Predicted response
$\beta_0$	Constant
$\beta_i$	Coefficients of linear
$\beta_{ii}$	Coefficients of quadratic
$\beta_{ij}$	Coefficients of interaction terms
$X$	Coded variables
$\varepsilon$	Error

## References

1. Zhou, J., Retraint, D., Sun, Z., et al. "Comparative study of the effects of surface mechanical attrition treatment and conventional shot peening on low cycle fatigue of a 316L stainless steel", *Surf. Coatings Technol.*, **349**(June), pp. 556–566 (2018).

2. Lu, K. and Lu, J. “Nanostructured surface layer on metallic materials induced by surface mechanical attrition treatment”, *Mater. Sci. Eng. A*, **375–377**(1-2 SPEC. ISS.), pp. 38–45 (2004).
3. Liu, G., Lu, J., and Lu, K. “Surface nanocrystallization of 316L stainless steel induced by ultrasonic shot peening”, *Mater. Sci. Eng. A*, **286**(1), pp. 91–95 (2000).
4. Bagheri, S. and Guagliano, M. “Review of shot peening processes to obtain nanocrystalline surfaces in metal alloys”, *Surf. Eng.*, **25**(1), pp. 3–14 (2009).
5. Lu, K. and Lu, J. “Surface nanocrystallization (SNC) of metallic materials—presentation of the concept behind a new approach”, *J. Mater. Sci. Technol.*, **15**(3), pp. 193–197 (1999).
6. Todaka, Y., Umemoto, M., and Tsuchiya, K. “Comparison of nanocrystalline surface layer in steels formed by air blast and ultrasonic shot peening”, *Mater. Trans.*, **45**(2), pp. 376–379 (2004).
7. Rakita, M., Wang, M., Han, Q., et al. “Ultrasonic shot peening”, *Int. J. Comput. Mater. Sci. Surf. Eng.*, **5**(3), p. 189 (2013).
8. Yarar, E., Erturk, A.T., and Karabay, S. “Dynamic finite element analysis on single impact plastic deformation behavior induced by SMAT process in 7075-T6 Aluminum Alloy”, *Met. Mater. Int.*, 0123456789 (2021).
9. Yarar, E. and Erturk, A.T. “A numerical investigation of a single-shot impact effects on plastic deformation of Titanium Alloys”, *Adv. Sci. Technol.*, **105**, pp. 119–124 (2021).
10. Hughes, D.A. and Hansen, N. “Deformation structures developing on fine scales”, *Philos. Mag.*, **83**(31–34), pp. 3871–3893 (2003).
11. Olugbade, T.O. and Lu, J. “Literature review on the mechanical properties of materials after surface mechanical attrition treatment (SMAT)”, *Nano Mater. Sci.*, **2**(1), pp. 3–31 (2020).
12. Sun, Z., Restraint, D., Baudin, T., et al. “Experimental study of microstructure changes due to low cycle fatigue of a steel nanocrystallised by Surface Mechanical Attrition Treatment (SMAT)”, *Mater. Charact.*, **124**, pp. 117–121 (2017).
13. Anand Kumar, S., Ganesh Sundara Raman, S., and Sankara Narayanan, T.S.N. “Effect of surface mechanical attrition treatment on fatigue lives of alloy 718”, *Trans. Indian Inst. Met.*, **65**(5), pp. 473–477 (2012).
14. Kang, X., Wang, T., and Platts, J. “Multiple impact modelling for shot peening and peen forming”, *Proc. Inst. Mech. Eng. Part B J. Eng. Manuf.*, **224**(5), pp. 689–697 (2010).
15. Chaise, T., Li, J., Nélías, D., et al. “Modelling of multiple impacts for the prediction of distortions and residual stresses induced by ultrasonic shot peening (USP)”, *J. Mater. Process. Technol.*, **212**(10), pp. 2080–2090 (2012).
16. Astaraee, A.H., Miresmaeili, R., Bagherifard S., et al. “Incorporating the principles of shot peening for a better understanding of surface mechanical attrition treatment (SMAT) by simulations and experiments”, *Mater. Des.*, **116**, pp. 365–373 (2017).
17. Yin, F., Hua, L., Wang, X., et al. “Numerical modelling and experimental approach for surface morphology evaluation during ultrasonic shot peening”, *Comput. Mater. Sci.*, **92**, pp. 28–35 (2014).
18. Manchoul, S., Seddik, R., Grissa, R., et al. “A predictive approach to investigate the effect of ultrasonic shot peening on a high-cycle fatigue performance of an AISI 316L target”, *Int. J. Adv. Manuf. Technol.*, **95**(9–12), pp. 3437–3451 (2018).
19. Sun, Q., Han, Q., Xu, R., et al. “Localized corrosion behaviour of AA7150 after ultrasonic shot peening: Corrosion depth vs. impact energy”, *Corros. Sci.*, **130**(November 2017), pp. 218–230 (2018).
20. Du, H., Wei, Y., Zhang, H., et al. “Effect of velocity of balls on the strain and stress of low carbon steel surface layer during SMAT”, *Int. J. Mod. Phys. B*, **23**, pp. 1924–1930 (2009).
21. Pilé, C., François, M., Restraint, D., et al. “Modelling of the ultrasonic shot peening process”, *Mater. Sci. Forum*, **490–491**, pp. 67–72 (2005).
22. Micoulaud, M., Mechkov, S., Restraint, D., et al. “Granular gases in mechanical engineering: On the origin of heterogeneous ultrasonic shot peening: Granular gases in mechanical engineering”, *Granul. Matter*, **9**(1–2), pp. 25–33 (2007).
23. Badreddine, J., Rouhaud, E., Micoulaud, M., et al. “Simulation of shot dynamics for ultrasonic shot peening: Effects of process parameters”, *Int. J. Mech. Sci.*, **82**, pp. 179–190 (2014).
24. Rousseau, T., Hoc, T., Gilles, P., et al. “Effect of bead quantity in ultrasonic shot peening: Surface analysis and numerical simulations”, *J. Mater. Process. Technol.*, **225**, pp. 413–420 (2015).
25. Bahl, S., Suwas, S., Ungàr, T., et al. “Elucidating microstructural evolution and strengthening mechanisms in nanocrystalline surface induced by surface mechanical attrition treatment of stainless steel”, *Acta Mater.*, **122**, pp. 138–151 (2017).
26. Tsai, M.T., Huang, J.C., Tsai, W.Y., et al. “Effects of ultrasonic surface mechanical attrition treatment on microstructures and mechanical properties of high entropy alloys”, *Intermetallics*, **93**, pp. 113–121 (2018).
27. Li, K., Spartacus, G., Dong, J., et al. “Effect of ultrasonic shot peening on microstructure and properties of 301SS”, *Mater. Manuf. Process.*, **32**(16), pp. 1851–1855 (2017).

28. Kumar, S., Chattopadhyay, K., and Singh, V. “Effect of ultrasonic shot peening on LCF behavior of the Ti-6Al-4V alloy”, *J. Alloys Compd.*, **724**, pp. 187–197 (2017).
29. Gallitelli, D., Reirant, D., and Rouhaud, E. “Comparison between conventional shot peening (SP) and surface mechanical attrition treatment (SMAT) on a titanium alloy”, *Adv. Mater. Res.*, **996**, pp. 964–968 (2014).
30. Pandey, V., Chattopadhyay, K., Santhi Srinivas, N.C., et al. “Role of ultrasonic shot peening on low cycle fatigue behavior of 7075 aluminium alloy”, *Int. J. Fatigue*, **103**, pp. 426–435 (2017).
31. Olugbade, T. and Lu, J. “Characterization of the corrosion of nanostructured 17-4 PH stainless steel by Surface Mechanical Attrition Treatment (SMAT)”, *Anal. Lett.*, **52**(16), pp. 2454–2471 (2019).
32. Olugbade, T.O. “Electrochemical characterization of the corrosion of mild steel in saline following mechanical deformation”, *Anal. Lett.*, **52**, pp. 2454–2471 (2020).
33. Olugbade, T. and Lu, J. “Enhanced corrosion properties of nanostructured 316 stainless steel in 0.6 M NaCl solution”, *J. Bio-Tribo-Corrosion*, **5**(2), pp. 1–11 (2019).
34. Olugbade, T., Liu, C., and Lu, J. “Enhanced passivation layer by Cr diffusion of 301 stainless steel facilitated by SMAT”, *Adv. Eng. Mater.*, **21**(8), pp. 1–11 (2019).
35. Sun, H.Q., Shi, Y.N., and Zhang, M.X. “Wear behaviour of AZ91D magnesium alloy with a nanocrystalline surface layer”, *Surf. Coatings Technol.*, **202**(13), pp. 2859–2864 (2008).
36. Wen, L., Yuan, Y., Wang, Y., et al. “Effect of nanocrystalline surface and iron-containing layer obtained by SMAT on tribological properties of 2024 Al alloy”, *Xiyou Jinshu Cailiao Yu Gongcheng/Rare Met. Mater. Eng.*, **44**(6), pp. 1320–1325 (2015).
37. Liu, Y., Jin, B., Li, D.J., et al. “Wear behavior of nanocrystalline structured magnesium alloy induced by surface mechanical attrition treatment”, *Surf. Coatings Technol.*, **261**, pp. 219–226 (2015).
38. Chamgordani, A.S., Miresmaeili, R., and Aliofk-hazraei, M. “Improvement in tribological behavior of commercial pure titanium (CP-Ti) by surface mechanical attrition treatment (SMAT)”, *Tribol. Int.*, **119**, pp. 744–752 (2018).
39. Erturk, A.T., Vatanserver, F., Yazar, E., et al. “Effects of cutting temperature and process optimization in drilling of GFRP composites”, *J. Compos. Mater.*, **55**(2), pp. 235–249 (2021).
40. Yazar, E. and Karabay, S. “Investigation of the effects of ultrasonic assisted drilling on tool wear and optimization of drilling parameters”, *CIRP J. Manuf. Sci. Technol.*, **31**, pp. 265–280 (2020).
41. Erturk, A.T., Vatanserver, F., Yazar, E., et al. “Machining behavior of multiple layer polymer composite bearing with using different drill bits”, *Compos. Part B Eng.*, **176**(April), p. 107318 (2019).

## Biographies

**Eser Yazar** is a researcher in mechanical engineering at the University of Kocaeli and continues his PhD studies. He received his bachelor’s degree from the Department of Mechanical Engineering at Istanbul University and his master’s degree from the Department of Mechanical Engineering at Kocaeli University. His research interests are modeling and simulation, vibration, and manufacturing.

**Alpay Tamer Erturk**, born in 1981, is currently working in the Machine and Metal Technologies Department of Kocaeli University. He obtained his BSc, MSc, and PhD degrees in the Mechanical Engineering Department of Kocaeli University. Dr. Erturk has lectured on various engineering disciplines including Mechanical Engineering, Metallurgical & Materials Engineering, Mechatronics Engineering, and Electrical Engineering. His research interests include areas of materials processing, the strength of materials, wear, mechanical & chemical behavior, and the manufacturing & characterization of metallic foams and lattice structures.